Horsefly object-directed polarotaxis is mediated by a stochastically distributed ommatidial subtype in the ventral retina

Andrej Meglič[a,1], Marko Ilić[b,1], Primož Pirih[a], Aleš Škorjanc[a], Martin F. Wehling[c], Marko Kreft[a,d,e], and Gregor Belušič[a,2]

[a]Department of Biology, Biotechnical Faculty, University of Ljubljana, 1000 Ljubljana, Slovenia; [b]Laboratory of Neuroethology, Sokendai – The Graduate University for Advanced Studies, 240-0193 Hayama, Japan; [c]Nature-inspired Team, Sensor and Imaging Sciences Branch, Air Force Research Laboratory, Eglin Air Force Base, FL 32542, [d]Institute of Pathophysiology, Faculty of Medicine, University of Ljubljana, 1000 Ljubljana, Slovenia; and [e]Celica Biomedical, 1000 Ljubljana, Slovenia

Edited by Claude Desplan, New York University, New York, NY, and approved September 11, 2019 (received for review June 24, 2019)

The ventral compound eye of many insects contains polarization-sensitive photoreceptors, but little is known about how they are integrated into visual functions. In female horseflies, polarized reflections from animal fur are a key stimulus for host detection. To understand how polarization vision is mediated by the ventral compound eye, we investigated the band-eyed brown horsefly *Tabanus bromius* using anatomical, physiological, and behavioral approaches. Serial electron microscopic sectioning of the retina and single-cell recordings were used to determine the spectral and polarization sensitivity (PS) of photoreceptors. We found 2 stochastically distributed subtypes of ommatidia, analogous to pale and yellow of other flies. Importantly, the pale analog contains an orthogonal analyzer receptor pair with high PS, formed by an ultraviolet (UV)-sensitive R7 and a UV- and blue-sensitive R8, while the UV-sensitive R7 and green-sensitive R8 in the yellow analog always have low PS. We tested horsefly polarotaxis in the field, using lures with controlled spectral and polarization composition. Polarized reflections without UV and blue components rendered the lures unattractive, while reflections without the green component increased their attractiveness. This is consistent with polarotaxis being guided by a differential signal from polarization analyzers in the pale analogs, and with an inhibitory role of the yellow analogs. Our results reveal how stochastically distributed sensory units with modality-specific division of labor serve as separate and opposing input channels for visual guidance.

polarization vision | rhabdomere | insect photoreceptor | retinal mosaic | pale

Linearly polarized light is exploited by many terrestrial animals as an important celestial navigational cue (1, 2). On the other hand, some animals use polarization vision to enhance the visual contrast (3–5). Horseflies are attracted to linearly polarized light, reflected from natural or man-made objects (6, 7). Females and males use the polarized reflections from the surface of water bodies to locate water for oviposition and mating, respectively. To produce and lay eggs, the females require a blood meal from mammalian hosts (8). They are attracted to polarized light reflected from shiny animal fur, which helps them to discern the dark silhouettes of host animals from the visual clutter in the natural environment (9). The attraction of horseflies to objects reflecting polarized light, the "positive polarotaxis," is driven by the degree of polarization and is independent of the polarization angle (7). To unravel the neural substrate for horsefly polarotaxis, we have studied the anatomical and physiological properties of the retina of the female band-eyed brown horsefly, *Tabanus bromius*, and tested our findings with behavioral experiments in the field.

Horseflies (family Tabanidae) belong to the higher flies (Diptera: Brachycera). Their retina is composed of several hundreds to thousands of optical units, the ommatidia (10). Extensive studies on higher flies revealed that each ommatidium is composed of 8 photoreceptor or retinula (R) cells. These cells detect the incoming light with light-guiding organelles (11), the rhabdomeres. The rhabdomeres of the 6 outer or peripheral photoreceptors (R1 through R6, R1–6) act as spatially and optically separated light guides, while the rhabdomeres of the 2 inner or central photoreceptors (R7 and R8) form an isolated, tiered light guide in the center of the ommatidium, with R7 occupying the distal and R8 the proximal part (12). The "open rhabdom" with separated rhabdomeres is associated with the sophisticated photoreceptor–interneuron wiring scheme of the neural superposition eye of flies (13).

The fly photoreceptors R1–6, which terminate in the first optical neuropil, the lamina (14, 15), have the same spectral sensitivity, extending from the ultraviolet (UV) into the green wavelength range (10, 16). They mediate achromatic and motion vision (17, 18). The photoreceptors R7 and R8 terminate in the second optical neuropil, the medulla (15, 19). They have narrow-band spectral sensitivities and mediate color and polarization vision (20–22). The functions of R1–6 and R7 and R8 nevertheless partially overlap (23, 24). Fly photoreceptors R7 are most sensitive to UV light. They occur in tandem with a blue-sensitive R8 photoreceptor in ommatidia termed "pale" and with a green-sensitive R8 in ommatidia termed "yellow," thus yielding 2 sets of central photoreceptors: R7p, R8p and R7y, R8y (25). In fruitflies,

Significance

Insect compound eyes are a random array of 2 or more subtypes of optical units, the ommatidia. Some ommatidia may contain photoreceptors sensitive to polarized light, but their functional integration into the visual system has not been explained. Here, we report that horsefly retina contains 2 ommatidial subtypes that separately analyze polarization of light and color. Horseflies seek their prey by detecting polarized reflections from animal fur. We explain why horseflies are attracted to shiny and to blue objects. Understanding this mechanism will help in controlling fly disease vectors. This study gives an explanation for ommatidial subtype specialization that goes beyond color vision and which is likely a common feature of many insect eyes.

Author contributions: A.M., M.I., M.F.W., and G.B. designed research; A.M., M.I., P.P., A.Š., M.F.W., M.K., and G.B. performed research; A.M., M.I., and G.B. analyzed data; and A.M., M.I., P.P., and G.B. wrote the paper.

The authors declare no competing interest.

This article is a PNAS Direct Submission.

Data deposition: The original image stack of horsefly retina serial block-face scanning electron micrographs is available as raw images (high-resolution tiff) and movies at Figshare, https://dx.doi.org/10.6084/m9.figshare.8222444.

[1]A.M. and M.I. contributed equally to this work.

[2]To whom correspondence may be addressed. Email: gregor.belusic@bf.uni-lj.si.

This article contains supporting information online at www.pnas.org/lookup/suppl/doi:10.1073/pnas.1910807116/-/DCSupplemental.

First published October 7, 2019.

houseflies, and blowflies, the 2 ommatidial subtypes are distributed stochastically (26), while in, for example, long-legged flies they may occur in ordered patterns (27, 28). In the marginal row of ommatidia in the fly dorsal retina, the dorsal rim area (DRA), both R7 and R8 are UV-sensitive (29, 30) and mediate the detection of polarized light from the sky (31, 32).

Each rhabdomere is composed of tens of thousands of microvilli. The microvilli are intrinsically dichroic, meaning that the probability of photon absorption depends on the photon's electric field vector, the e-vector. The ratio of maximal to minimal absorption probabilities is termed the microvillar dichroic ratio, D_m (33–36). Photoreceptors having rhabdomeres with ordered microvilli, all occupying a single orientation, can achieve a high polarization sensitivity (PS). High PS can, however, result in the detection of polarization-dependent contrasts, thereby confounding achromatic and color vision (37–39). To avoid the polarization-dependent artifacts, many insect photoreceptors minimize their PS by rotating or twisting their microvilli along the rhabdomere (37, 40–43). On the other hand, photoreceptors optimized for high PS have aligned microvilli and short rhabdomeres with little self-screening (44). Photoreceptors with aligned, "untwisted" microvilli, short rhabdomeres, and high PS occur mostly in specialized areas, such as the DRA. Notably, the R7 and R8 photoreceptors in the DRA of horseflies have interdigitated rhabdomeres with orthogonally arranged microvilli, similar to crustaceans. This anatomical configuration reduces self-screening and thus combines high photon capture with high PS (44, 45). The sophisticated DRA indicates that the horseflies also utilize celestial polarization vision for navigation.

Another particular feature of the horsefly compound eye is that the R7 and R8 photoreceptors in the central and ventral retina have untwisted rhabdomeres (46, 47). The distal R7 occupies about 60% and the proximal R8 about 40% of the common waveguide, close to the morphological measurements from the DRA and the modeled optimum for polarization vision at medium light intensities (48). These cells are thus excellent candidates for horsefly ventral polarization vision (VPV). Photoreceptors with high PS have also been found in the ventral retina in a limited number of other insect species (27, 42, 49–52). In *Drosophila*, VPV is mediated by R7 photoreceptors with untwisted rhabdomeres residing in a subset of pale ommatidia, perhaps in combination with a subclass of R1–6 having little rhabdomeric twist (42). In all these cases, VPV has been associated with the detection of water surfaces that produce horizontally polarized reflections.

The blueprint for color or polarization vision is based upon photoreceptors that sample a common point in the visual space, having different spectral or polarization sensitivities. Their outputs are compared by so-called opponent processing that takes place in the receptor axons (53, 54) or in the interneurons (55). In order to avoid the confusion between the spectral composition of incident light and its degree or angle of linear polarization, the photoreceptors mediating polarization vision should express the same rhodopsins, as is the case in the DRA (31, 56).

We have characterized the photoreceptors in the frontal ventral retina of the female horsefly by assessing the twisting of the microvilli in a large sample of ommatidia using serial sectioning and by measuring their spectral and polarization sensitivities using sharp microelectrode recordings. The results allowed us to formulate hypotheses for field experiments, where we tested horsefly polarotactic behavior by manipulating the spectral and polarization composition of artificial lures. This study reveals the complex interplay of photoreceptor classes and ommatidial types that mediate the visual guidance of polarotactic horseflies and provides clues about the mechanisms driving the visual behavior of biting flies.

Results

Anatomy. We first analyzed "rhabdomeric twisting," the change in orientation angle of the microvilli along the whole length of the rhabdomeres, in the frontal ventral retina of a female horsefly by serial block-face scanning electron microscopy (SBFSEM) (Fig. 1). The sample area, imaged with a longitudinal resolution of 5 μm, contained 15 ommatidia with 120 photoreceptors. The microvilli in the outer photoreceptors R1–6 in all ommatidia were aligned along the distal 100 μm but performed a 120° to 180° twist along the proximal 150 μm (Fig. 1 *B–E*).

The ommatidia were classified into 2 types, H and V, based on the horizontal (H; parallel to the eye equator) or vertical (V; perpendicular to the eye equator) orientation of the distal microvilli in the central photoreceptor R7 (Fig. 1*A*). Consequently, the 2 inner photoreceptors of the 2 ommatidial types were labeled as R7H, R8H, and R7V, R8V. The R7H and R7V could be also distinguished with light microscopy (*SI Appendix*, Fig. S1*B*). Thus, we were able to map the ommatidial types across the retina. The H- and V-type ommatidia are distributed semi-stochastically, with a dorsal-to-ventral gradient: the ventral and ventrolateral retina contains up to 72% H and 28% V ommatidia, while the dorsal retina contains up to 37% H and 63% V ommatidia (*SI Appendix*, Fig. S1 *A–D*).

In the H-type ommatidia, the microvilli of both R7H and R8H remain aligned along the entire length of the rhabdomere (Fig. 1*B*); those in R7H twist slightly from the horizontal axis by <30°, but those in R8H remain vertically aligned (Fig. 1*F*). This means that the microvilli of R7H and R8H together constitute an orthogonal analyzer pair, suitable for polarization vision. In the V-type ommatidia, the microvilli of R7V and R8V remain mostly vertical along the distal half but twist by ∼90° along the proximal half of the rhabdomere (Fig. 1 *C* and *G*). The rhabdomeric twist is shown in Movies S1–S3.

Using the measured twisting of the rhabdomeres and assuming the microvillar dichroic ratio $D_m = 10$, we numerically modeled the anatomy-based PS (PS_A) of the photoreceptors and calculated their angular absorption maximum ϕ_{max}, that is, the e-vector angle with maximal absorption probability. The twisting almost abolishes the PS_A of the R1–6 ($PS_A = 1.1 \pm 0.1$). In the shorter and less-twisted R7V and R8V, the $PS_A \approx 2$. The angular absorption maxima were vertical ($\phi_{max} \approx 90°$) in R7V and R8V but could not be reliably calculated for R1–6. A high PS_A and horizontal angular absorption maximum were calculated for R7H ($PS_A \approx 5$, $\phi_{max} \approx 0°$). In R8H, the ϕ_{max} was vertical ($\phi_{max} \approx 90°$) and the PS_A was even higher than in R7H ($PS_A \approx 6$), due to the high alignment of the microvilli, the short length of the rhabdomere, and the distally located R7H, acting as a polarization filter.

Given their high calculated PS_A, we hypothesized that the central photoreceptors in the H-type ommatidia, R7H and R8H, mediate VPV in the female horsefly. The twisted rhabdomeres of R7V and R8V cause a reduced PS_A and the central photoreceptors of V-type ommatidia thus seem to be designated for color vision with minimal polarization artifacts. We note here that the central rhabdomeres could not be classified as pale and yellow with optical methods as in the housefly (26) (*SI Appendix*, Fig. S1 *E* and *F*).

Electrophysiology. The photoreceptors in the female horsefly retina were further characterized with intracellular recordings. The tracheolar sheath surrounding the ommatidia rendered the intracellular recordings quite challenging. The impalements did not last sufficiently long to allow for the identification of the penetrated cells via iontophoretic injection of dyes. Instead, the impaled cells (in >200 animals) were identified on the basis of their receptor potential, input resistance, and spectral and polarization sensitivity (*SI Appendix*, Fig. S2). The most frequently encountered photoreceptors (>300 impaled cells) had fast and smooth receptor

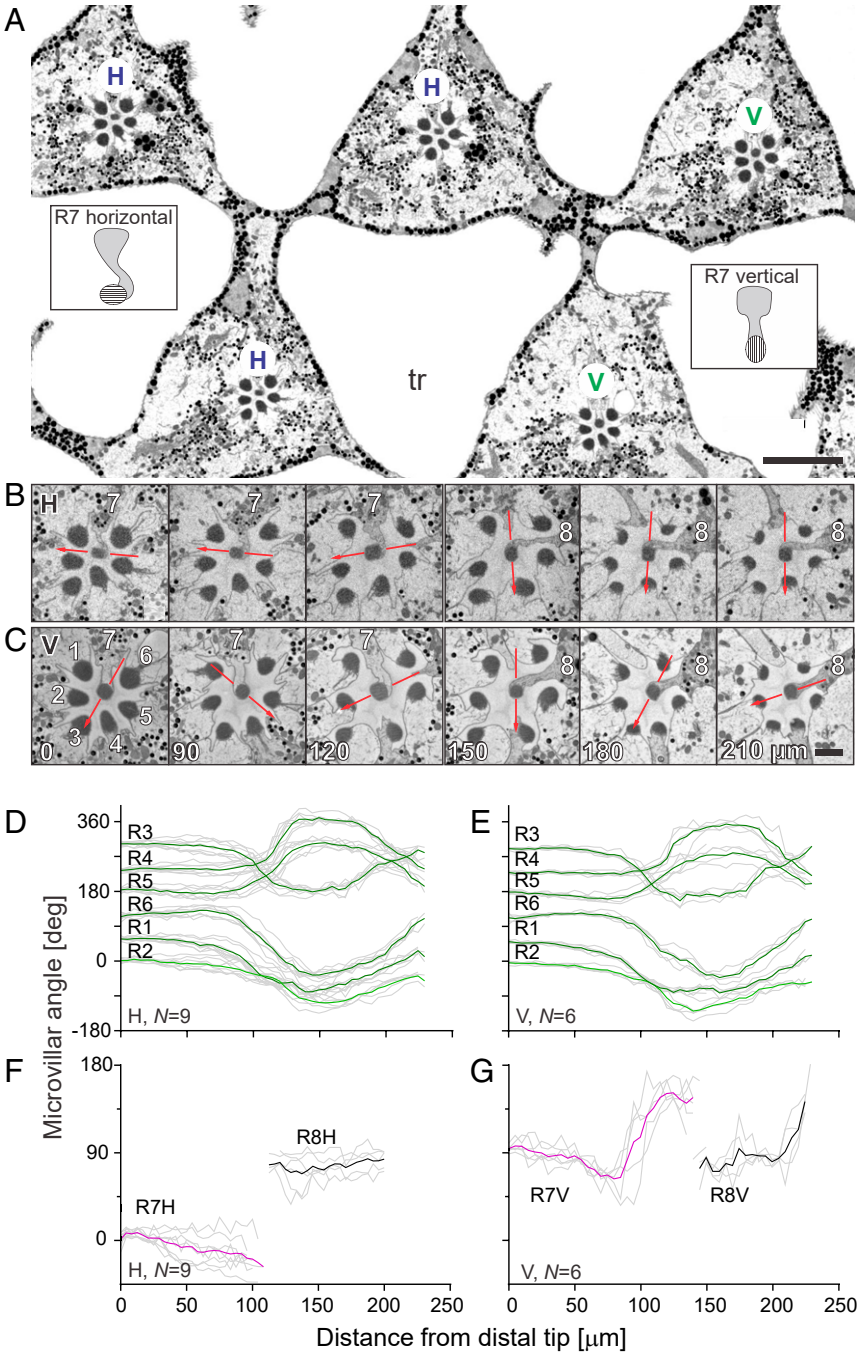

Fig. 1. Anatomical analysis of rhabdomeric twisting in the frontal ventral retina. (*A*) Block surface scan of the distal retina with triangular ommatidia separated by large tracheoles (tr); the ommatidia are labeled according to the vertical (V) or horizontal (H) alignment of the microvilli in the central photoreceptor R7 (schematized in insets). (Scale bar, 10 µm.) (*B* and *C*) An H and a V ommatidium at depths, indicated in micrometers in *C*. Red lines indicate orientation of R7 and R8 microvilli. Photoreceptor identity is indicated with numbers. (Scale bars, 1 µm.) (*D*–*G*) Microvillar angle in rhabdomeres R1–6 (*D* and *E*) and R7 and R8 (*F* and *G*) as a function of the distance from the distal tip in the 15 analyzed ommatidia of type H (*D* and *F*) and type V (*E* and *G*). In *D*–*G*, colored and black lines indicate group means and gray lines individual rhabdomeres. *N* indicates the number of analyzed rhabdomeres.

potentials, low input resistance, broad spectral sensitivity peaking in the green at 520 nm, and negligible PS (Fig. 2*A*). Those were identified as R1–6. Cells with slower, noisier receptor potentials, higher input resistance, and narrower spectral sensitivity (Fig. 2 *B*–*E*) were encountered much less frequently (~30 impaled cells, yielding 20 cells with full datasets). Those cells were identified as the central photoreceptors, R7 and R8.

We found 2 types of central photoreceptors with high PS and angular PS maxima that matched the anatomically determined ϕ_{max} and the PS_A of the central photoreceptors in H-type ommatidia. The type with maximal sensitivity in the UV ($\lambda_{max} \approx 360$ nm) and high PS and horizontal angular maximum (PS = 4.7 ± 1.7, $\phi_{max} \approx 0°$, $n = 3$) was identified as R7H. The type with maximal sensitivity in the UV and blue ($\lambda_{max} \approx 360$, 440 nm) and even higher PS and vertical angular maximum (PS = 8.0 ± 4.3, $\phi_{max} \approx 90°$, $n = 9$) was identified as R8H.

Additionally, we found 2 types of cells with low PS and vertical angular maximum that matched the expected values for the central

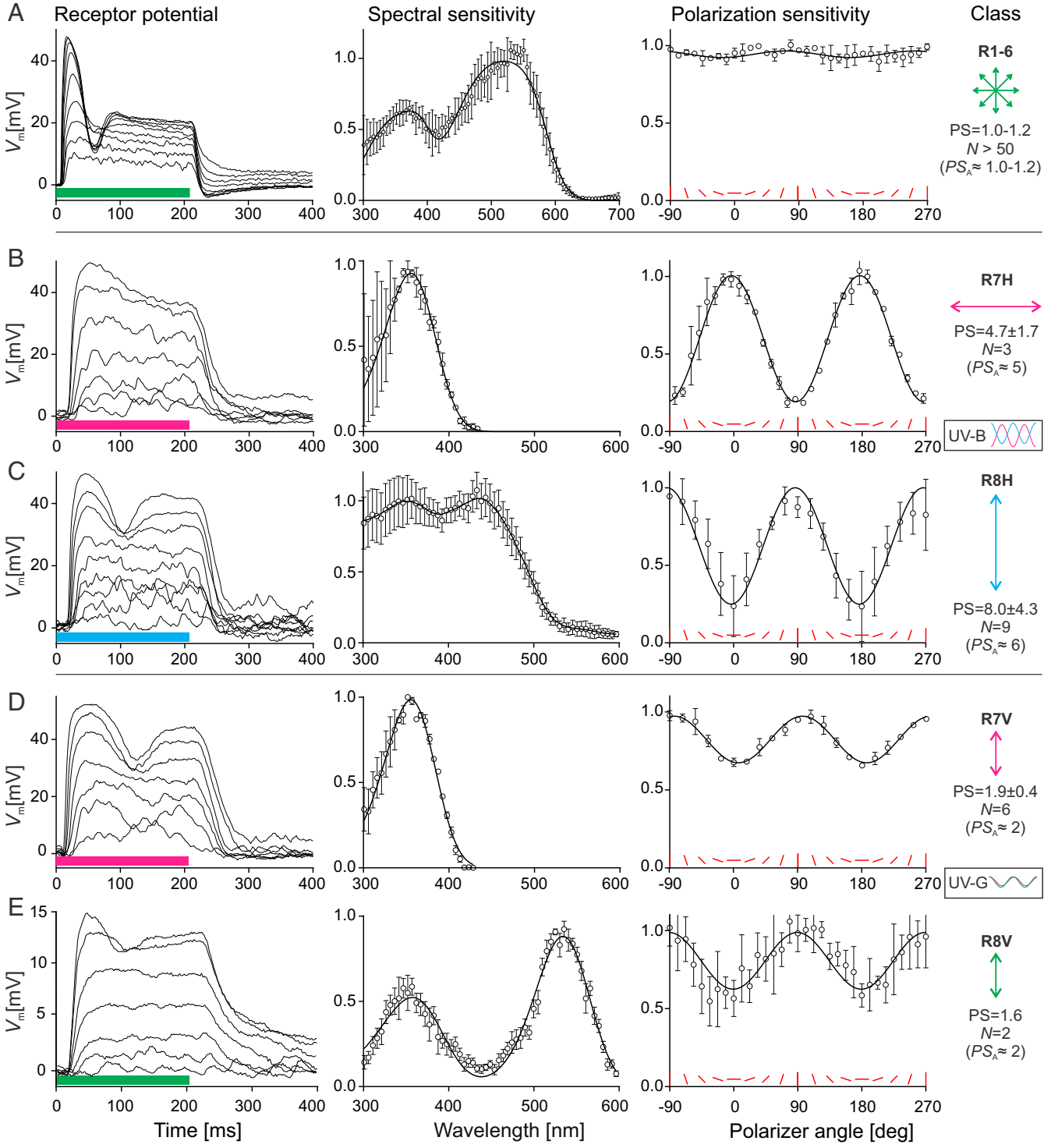

Fig. 2. Spectral and polarization sensitivity of the photoreceptors in the ventral retina. (*Left*) Receptor potentials, evoked by a series of pulses of UV, blue, or green light with graded intensity (360, 440, and 525 nm; pulses indicated by color bar below traces). (*Middle*) Averaged spectral sensitivities (mean ± SD), fitted with rhodopsin templates (*A, B, D,* and *E*; see *Materials and Methods*) or smoothed (*C*). (*Right*) Representative polarization sensitivities (data from multiple polarizer runs; mean ± SD), fitted with a squared cosine function; red bars indicate polarizer angle with respect to the eye equator. (*A*) Outer photoreceptors R1–6 with fast receptor potential, broad spectral sensitivity, and negligible PS. (*B–E*) Inner photoreceptors with slow and noisy receptor potential and narrower spectral sensitivity. Those with high PS (*B* and *C*) form orthogonal pairs of UV-sensitive R7H (*B*; maximal sensitivity to horizontally polarized light) and UV- and blue-sensitive R8H (*C*; maximal sensitivity to vertically polarized light), and those with low PS form parallel pairs of UV-sensitive R7V (*D*) and UV- and green-sensitive R8V (*E*), both with maximal sensitivity to vertically polarized light. At the right margin, the electrophysiologically measured PS is indicated together with the PS_A. Insets depict the spectral and polarization sensitivity of R7 and R8 receptor pairs in H- and V-type ommatidia, as inferred from the anatomy and electrophysiology.

photoreceptors in V-type ommatidia. The type with maximal sensitivity in the UV ($\lambda_{max} \approx 360$ nm; PS = 1.9 ± 0.4, $\phi_{max} \approx 90°$, $n = 6$) and the type with maximal sensitivity in the UV and green ($\lambda_{max} \approx 360$, 530 nm, $\phi_{max} \approx 90°$, $n = 3$; PS = 1.6, $n = 2$) were identified as R7V and R8V, respectively.

Behavioral Experiments. To assess the functional roles of the different photoreceptor classes and ommatidial types in horsefly visual guidance, we performed a series of field experiments with artificial lures (Figs. 3 and 4). Horseflies were lured with shiny black beach balls, reflecting light, polarized under all angles (*SI Appendix*, Fig. S3). The balls were suspended below UV-transmitting transparent plates (lure name "shiny UBG"; transmitting UV, blue, and green light) or below transparent plates with long-pass (cutoff at 400 nm, "BG"; cutoff at 450 nm, "G") and band-pass (maximal transmission at 450 ± 50 nm, "B") filters, chosen on the basis of spectral sensitivities of R7 and R8 photoreceptors (Fig. 3 *A* and *B*). A matte black ball, suspended below a UV-transmitting transparent plate served as a nonpolarized reference lure ("matte UBG"). Spectral combinations that were not possible with readily available filters were achieved with a light source that allowed separate control of the UV, blue, and green reflections (Fig. 4*A*). The attraction to the different lures was quantified by counting horsefly visits in 15-min episodes in several sessions; following each session, the lures were randomly exchanged.

UV and blue are necessary to trigger polarotaxis. The shiny G and matte UBG lures were both visited equally, but much less frequently than the shiny UBG (Fig. 3*C*). This suggests that UV- and blue-polarized light that stimulates R7H and R8H is necessary to trigger horsefly polarotaxis (Fig. 3*D*).

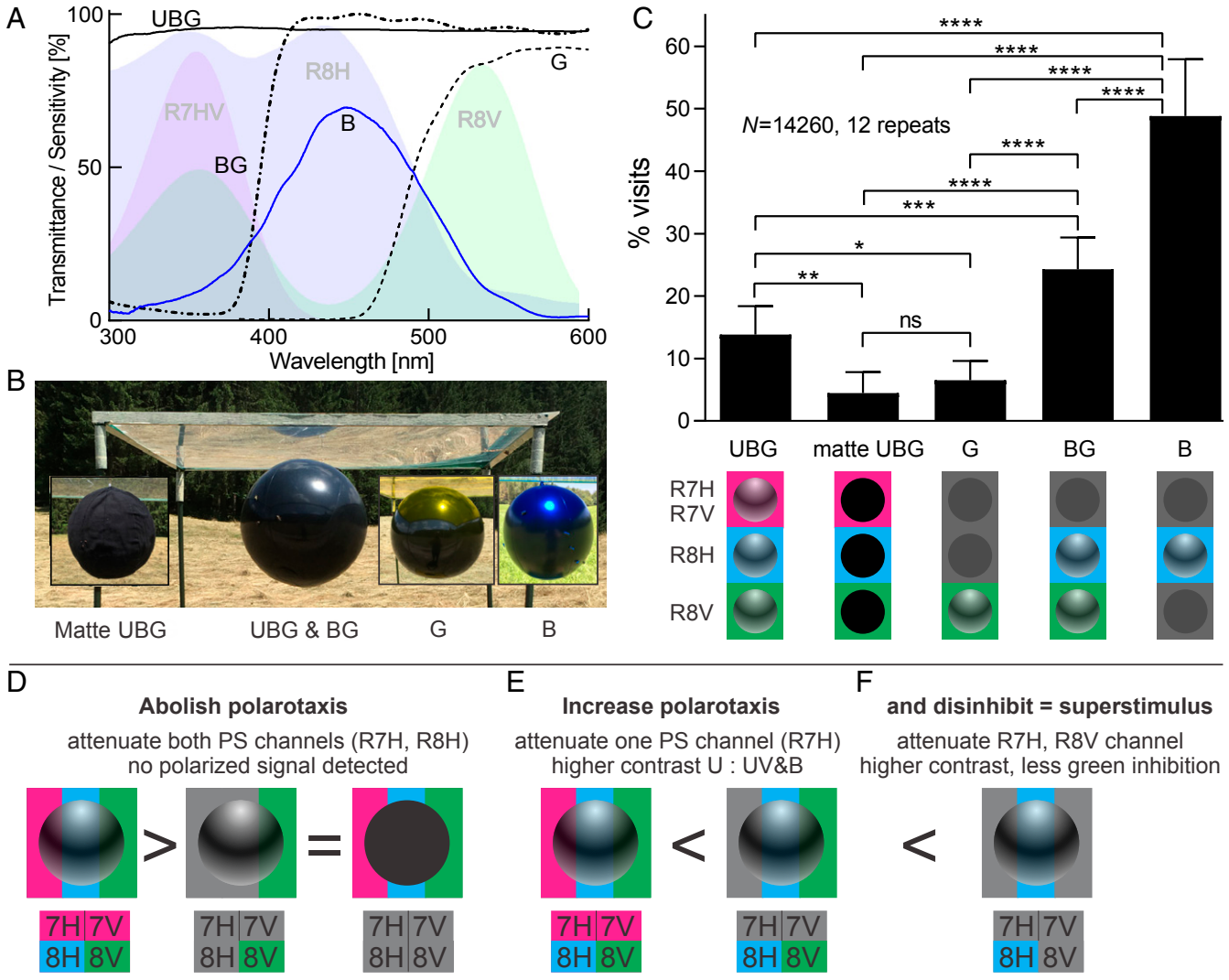

Fig. 3. Polarotactic behavior depends on the spectral composition of polarized light. (*A*) Transmittance of the filters used to control the spectra of light reflected from the black spheres (solid and dashed lines), together with the spectral sensitivities of the central photoreceptors (shaded areas: R7H and R7V, dark violet; R8H, light blue; R8V, light green). Full-spectrum filter, UBG (transmitting UV, blue B, and green G); UV cutoff filter, BG (transmitting B and G); UV and blue cutoff, G (transmitting G); blue bandpass, B (transmitting B). (*B*) RGB photograph of the combinations of spheres and filters. (*C*) Relative numbers of horsefly visits to the shiny balls reflecting full-spectrum polarized light (UBG), green polarized light (G), blue- and green-polarized light (BG), and blue-polarized light (B), compared to nonpolarized control (matte UBG). *$P < 0.05$, **$P < 0.01$, ***$P < 0.001$, ****$P < 0.0001$, not significant (ns) ($P > 0.05$) (Bonferroni-corrected Student's *t* test). (*D–F*) Interpretation of experimental results (*D*) Attenuation of reflected UV and B reduces the signal in all central photoreceptors except R8V; hence, a yellow-reflecting ball is equally as unattractive as a matte ball, which reflects no polarized light. (*E*) Attenuation of reflected UV enhances the difference in excitation within the orthogonal analyzer receptor pair of R7H and R8H, leading to increased polarotaxis. (*F*) Attenuation of reflected UV and G simultaneously increases the differential signal in the polarization analyzer pair and reduces the excitation in R8V, thereby increasing the polarotaxis and decreasing the inhibition by long-wavelength light.

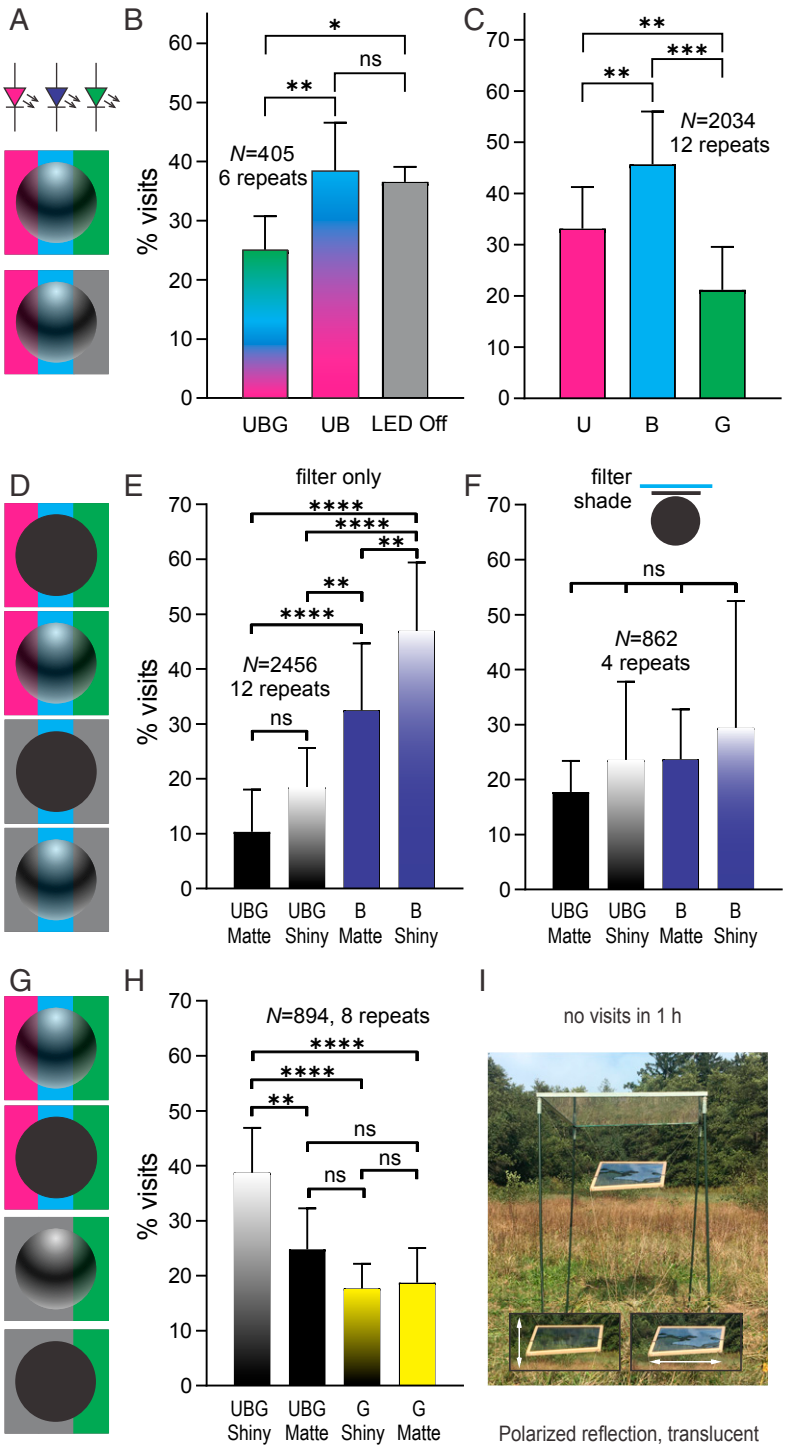

Fig. 4. Control behavioral experiments. (*A*–*C*) Attractiveness of polarized reflections, created by artificial illumination. (*A*) Shiny spheres, suspended below B and G LED strips and below UV fluorescent lamps. (*B*) Relative numbers of horsefly visits to spheres reflecting UBG, UB without G, or a sphere under lights off. Horseflies preferred UB over UBG. (*C*) Relative numbers of horsefly visits to spheres reflecting monochromic UV, B, or G light. Horseflies preferred monochromic B over UV and G. (*D*–*F*) Attractiveness of polarized and unpolarized monochromic B reflections. (*D*) Matte and shiny spheres, suspended below UBG or B filters, reflecting unpolarized and polarized UBG or B light. (*E*) Relative numbers of horsefly visits to spheres reflecting unpolarized (matte) or polarized (shiny) full-spectrum (UBG) or blue (B) light. Horseflies preferred the B-illuminated spheres, irrespective of polarization. (*F*) Relative numbers of horsefly visits to matte and shiny spheres, visually decoupled from the spectral filters by a cardboard shade. All shaded spheres were equally visited, indicating that the attraction in *E* was not caused by the presence of the spectral filters, but by reflected filtered light. (*G* and *H*) Attractiveness of spheres, reflecting polarized or unpolarized, long-wavelength (G or yellow) light. (*G*) Matte and shiny spheres, suspended below UBG and G filters, reflecting unpolarized or polarized UBG or G light. (*H*) Relative numbers of horsefly visits to spheres, reflecting unpolarized (matte) or polarized (shiny) full-spectrum (UBG) or green (G) light. Spheres below G are equally unattractive as the matte UBG; all received significantly fewer visits than a shiny UBG. G light inhibits the taxis, irrespective of degree of polarization. (*I*) Polarized reflection alone, without luminance contrast, created by obliquely suspended celluloid foil. (*Inset*) The foil, imaged through a polarization filter at 2 orientations, indicated by arrows. The object did not receive any horsefly visits during 1-h observation time. $*P < 0.05$, $**P < 0.01$, $***P < 0.001$, $****P < 0.0001$, not significant (ns) ($P > 0.05$) (Bonferroni-corrected Student's *t* test).

Cutting off UV increases polarotaxis. The shiny BG lure was visited almost twice more frequently than the shiny UBG lure (Fig. 3*C*). We presume that cutting off UV light in the case of the shiny BG lure caused the reflections to stimulate the UV- and blue-sensitive R8H, but not the UV-sensitive R7H, thus evoking a larger differential signal in the orthogonal analyzer receptor pair (Fig. 3*E*). From the perspective of the horsefly, a reflection lacking a UV component is confounded with one having a high degree of polarization.

Cutting off both UV and G creates a superstimulus. The shiny B lure received many more visits than both the shiny BG and shiny UBG lures (Fig. 3*C*). Similar to shiny BG, the blue-reflecting lure likely caused an increased differential signal detected by R7H and R8H. Additionally, as the V-type central receptor pair is completely blind to blue light (Fig. 2 *D* and *E*), the blue filter abolished any signal in the V-type ommatidia.

These 3 experiments together suggest that horsefly polarotaxis is regulated by interommatidial opponent interactions between the excitatory signal from the H-type and the inhibitory signal from the V-type ommatidia. We conclude that quasi-monochromic blue light is a superstimulus for the polarotactic horseflies (Fig. 3*E*).

Green light inhibits polarotaxis. When illuminated with artificial light sources, the balls reflecting UV, B, and G received fewer visits than those reflecting only UV and B (Fig. 4*B*). G light in polarized reflections inhibits polarotaxis, probably via excitation of R8V.

Monochromic UV is less attractive than monochromic blue. When presented with balls reflecting monochromic light, horseflies most frequently visited those reflecting B, less those reflecting UV, and even less those reflecting G light (Fig. 4*C*). Monochromic UV cannot lead to an increased contrast in the orthogonal analyzer pair, as both R7H and R8H are sensitive to UV, while only R8H is sensitive to B.

Monochromic blue is a superstimulus, irrespective of polarization. To test the dependence of attraction to B light on polarization, we compared the attractiveness of matte B vs. shiny B and used matte UBG and shiny UBG as controls (Fig. 4*D*). While the horseflies were most attracted to the polarized shiny B and least attracted to the unpolarized matte UBG lures, they still preferred the unpolarized matte B over the polarized shiny UBG (Fig. 4*E*). To exclude the possibility that the increased attraction to the matte B was caused by the blue filter itself, we visually decoupled the balls from the filters with a circular shade made from cardboard. Indeed, under these conditions the horseflies visited all lures equally (Fig. 4*F*).

Green is repelling, irrespective of polarization. To test the dependence of attraction to G light on polarization, we compared the attractiveness of matte G vs. shiny G lures and used matte UBG and shiny UBG lures as controls (Fig. 4*G*). Horseflies visited all 3 lures equally (Fig. 4*H*), indicating that in the absence of polarized reflections G light detected by R8V repels the horseflies, irrespective of variations in the short-wavelength spectrum of reflected light.

Polarization contrast without intensity contrast is insufficient to trigger polarotaxis. A polarized lure with minimal intensity contrast was created by obliquely suspended UV-transmitting celluloid foil, positioned at the same height as the black balls (Fig. 4*I*). We note that this lure was only horizontally polarized (*SI Appendix*, Fig. S3*B*), but horsefly polarotaxis is independent of the angle of polarization (7). This lure did not receive any visits, confirming that the polarotactically driven attack of the female horseflies is not triggered unless the polarized light is reflected from a dark object.

Discussion

Here, we have shown that the retina of female horseflies is built of 2 functionally segregated and semistochastically distributed ommatidial subtypes. In H-type ommatidia the central photoreceptors R7H and R8H have orthogonally oriented rhabdomeric microvilli and high PS; these ommatidia drive polarotaxis. The V-type ommatidia harbor central photoreceptors with parallel rhabdomeric microvilli and low PS; these ommatidia inhibit polarotaxis. Functional organization of the horsefly retina is a prime example of the evolutionary tuning of an ancestral sensory system—the compound eye—toward the solution of a specific problem, the detection of dark-furred, shiny animals and water surfaces against a background cluttered with polarization, intensity, and color contrast.

The spectral sensitivities of UV- and UV- and blue-sensitive polarization detectors indicate that the H-type ommatidia are analogous to fly pale ommatidia, while the UV and green receptors in V-type ommatidia indicate that these ommatidia are analogous to fly yellow ommatidia (25). Interestingly, the ratio of both ommatidial subtypes in the dorsal half of the retinal mosaic corresponds to the 0.3:0.7 pale:yellow ratio observed in *Drosophila melanogaster* (57); the inverse, 0.7:0.3 ratio in the ventral retina, however, exceeds the highest pale:yellow ratio observed in drosophilid flies (58), indicating that the ventral part of the eye is optimized for polarization vision.

The R7H rhabdomeres are exceptionally slender (*SI Appendix*, Fig. S4) and thus optimized for high-acuity vision (11, 59). This is in sharp contrast with the central rhabdomeres of polarization detectors in fly DRA that are usually much wider than their counterparts in the rest of the retina (32), resulting in increased acceptance angles (31). The central rhabdomeres are short, which allows high PS. Consequently, they harbor fewer visual pigment molecules and fewer transducing units, microvilli, than R1–6. As predicted by modeling (48), the transduction gain in R7 and R8 is set higher, which in combination with high input resistance causes large amplitudes of graded responses, but also higher voltage noise (*SI Appendix*, Fig. S2 *E*–*G*). Large voltage signals are likely required for efficient propagation of signals via the long fibers into the medulla.

We have previously shown that the contrast between the polarized patterns reflected from fur or water and the surrounding visual clutter is optimal in the UV- and blue-wavelength range (60). This has most likely driven the evolution of horsefly VPV to employ UV- and blue-sensitive photoreceptors. The shiny cuticles of leaves create a cluttered polarized background (61), which can be discerned from the prey or water using the yellow ommatidia that harbor the green-sensitive R8V photoreceptors. These inhibit the polarotaxis upon the detection of long-wavelength or green light from the vegetation, irrespective of its degree or angle of polarization.

Our study reveals the retinal mechanisms that likely support the visual guidance of polarotactic horseflies. The taxis is regulated by the opposing signals from the central photoreceptor pairs in the pale and yellow ommatidia, but the attack is only elicited upon the detection of a dark object, probably mediated by neural circuits downstream of R1–6 (Fig. 5).

The lures in behavioral experiments had greatly varying absolute radiances that depended on the time of the day, cloud cover, uneven terrain, and texture of the lure and the type of filter used. For instance, reflections from the most attractive lures (shiny BG and B) differed in intensity by at least an order of magnitude; the electric lamps that evoked horsefly responses were much weaker than any lure illuminated by the sky and the sun. Still, the horseflies reacted in a predictable way in all cases, indicating that they have evolved polarization and color vision that can cope with vast changes in light intensity.

Our study attributes a functional role to the insect retinal mosaic. In the main retina of the female horseflies it is composed of 2 segregated ommatidial populations, one dedicated to polarization vision and one to color vision. Interestingly, in *Drosophila*, color vision—at least in the blue-green range—is mainly mediated by the yellow ommatidia (23), while VPV ceases upon the silencing of the pale ommatidia (42). Thus, the basic functional roles of the ommatidial subtypes in the fly retinal mosaic seem to be highly conserved among the Diptera. Our study does not completely exclude the possibility that R7 and R8 from the ommatidia analogous

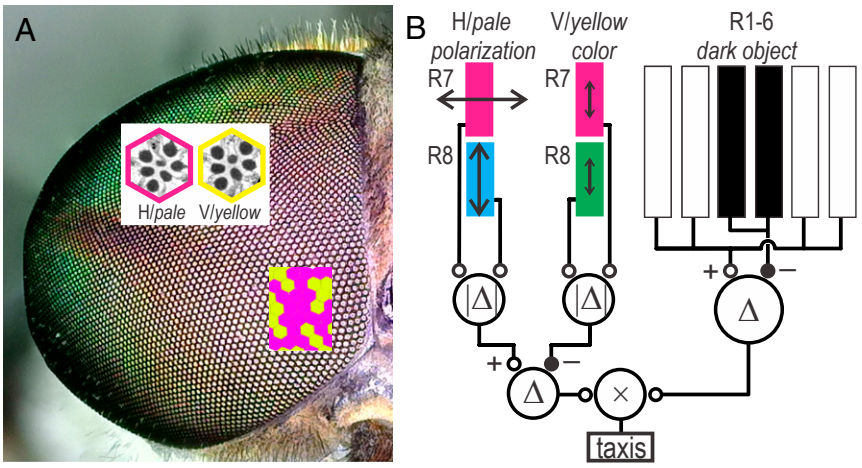

Fig. 5. Retinal substrate for visual guidance of polarotactic horseflies. (*A*) Compound eye of a *T. bromius* female is composed of a stochastic mosaic of ommatidia with horizontal (H) or vertical (V) distal microvilli of R7, analogous to the fly pale and yellow ommatidia. (*B*) Proposed scheme of horsefly visual guidance. Polarotactic attack of a horsefly, seeking a blood meal, is triggered by multistaged intraommatidial and interommatidial opponent processing of visual signals. The attack is facilitated by the short-wavelength polarized light, detected by the orthogonal analyzer pair of UV-sensitive R7 and UV- and blue-sensitive R8 in H or pale ommatidia, inhibited by the long-wavelength light, detected by the opponent pair of UV-sensitive R7 and UV- and green-sensitive R8 in V or yellow ommatidia. The attack is guided toward a dark object, which is detected by the outer photoreceptors R1–6 that sample the same direction in the visual space as the inner photoreceptors. |Δ|, rectified difference; Δ, difference; ×, multiplication.

to yellow contribute to polarization vision, as their PS was not negligible. In principle, R7H and R7V from adjacent ommatidia could also form polarization-opponent, orthogonal analyzer pairs, but this seems rather unlikely as their diverging visual axes would hinder their ability to reliably detect small polarized targets. Additionally, the 2 ommatidial subtypes frequently occur in clusters enriched only in a single V or H type (*SI Appendix*, Fig. S1*B*), rendering unlikely a common neural wiring for an inter-ommatidial opponent processing of polarization.

The spectral sensitivities of horsefly photoreceptors substantially differ from those in the other higher flies (Brachycera) (10). Horsefly R1–6 have spectral peak wavelengths in the green, similar to the R1–6 of lower flies (Nematocera) (62). The polarization analyzer pair of R7H and R8H strongly differs from that of DRA R7 and R8 in the fruitfly (29), housefly, or blowfly (30) DRA, where both cells express the same UV-sensitive rhodopsin Rh3 (29) and consequently form a homochromic pair. The horsefly's UV-sensitive R7H and UV- and blue-sensitive R8H form a spectrally imbalanced or heterochromic analyzer pair, similar as the one found in *Daphnia pulex* (63), which cannot be used to reliably distinguish polarization and color cues. Horseflies thus confound color and polarization, similar to papilionid butterflies (38, 39). Anyhow, the horsefly attraction to blue, man-made objects is most likely a new phenomenon. Interestingly, the affinity of tabanid flies to blue has been observed in various field experiments (64–66). For instance, blue hats coated with Tanglefoot have been traditionally used by North American fishermen to trap tabanid flies. Furthermore, traps that have high reflectance in the blue but low reflectance in the UV (similar to our lures underneath B filter) have proven to be optimal for trapping the blood-sucking tsetse flies (Glossinidae) (67) which also contain central photoreceptors with high PS in the ventral retina (68). Our study thus explains the mysterious affinity of biting higher flies (Brachycera) to blue objects (69) that is probably based on the heterochromic photoreceptor pairs evolved for VPV. Besides this, it seems that the perception of polarized reflections is not a separate modality but rather an integral part of horsefly color vision, where polarized clues might be perceived as blue patches.

Understanding object-directed polarization vision in tabanids will certainly be helpful for understanding polarization-assisted object vision and opponent coding in many visual animals. The functional organization of horsefly retina presents an example of an efficient mixed array of polarization, color, and intensity sensors that might offer a blueprint for advanced technical solutions in the context of artificial visual systems.

Materials and Methods

Animals. Horseflies were collected between May and September in the wetlands and in the hills south of Ljubljana, Slovenia. The insects were attracted by a black polyethylene sheet on the ground or by shiny car surfaces. They were individually stored in plastic containers and kept in a refrigerator. The species were identified following the local key (70). Approximately 80% were identified as *T. bromius*, ∼10% as *Tabanus bovinus*, and the remaining ∼10% as *Tabanus tergestinus* or *Chrysops caecutiens*. Anatomical and electrophysiological experiments were performed only in *T. bromius*, while all species from the genus *Tabanus* were included in the behavioral experiments.

Anatomy. The head of a female horsefly was hemisectioned and the eyes were isolated using a razor blade and microscissors. The air sacks in the head were removed to ensure a better penetration of the fixative. The eyes were in a light-adapted state, as the animals were exposed to light before and during isolation.

Samples for light microscopy and SBFSEM were prepared following the same protocol. Complete eyes were fixated for 3 h in 3.5% glutaraldehyde and 4% aldehyde in 0.1 M Na-cacodylate buffer (pH 7.2). After postfixation for 90 min at a room temperature in 1% OsO_4 in 0.1 M Na-cacodylate the specimens were rinsed in 0.1 M Na-cacodylate and distilled water, dehydrated in graded ethanol (50 to 100% in 10% steps) series, infiltrated in propylene oxide, and embedded in Spurr's resin (SPI). Semithin sections were made using a Histo diamond knife (Diatom), transferred to object slides, colored with Azur II (Sigma), and observed with an AxioImage Z1 microscope (Zeiss).

A sample of the frontal ventral retina of a female horsefly was analyzed with a serial block-face scanning electron microscope, based on an ESEM Quanta 600 FEG scanning electron microscope (FEI Company), fitted with a 3View ultramicrotome (Gatan) at the FELMI Institute in Graz, Austria. Resin-embedded tissues were mounted on aluminum specimen pins using cyanoacrylic glue and precision-trimmed with a diamond knife (Diatome). Silver paint was used to electrically ground the edges of the tissue block to the aluminum pin. The sample was cut in the *z* axis in 100-nm layers. Each 100-nm section was imaged at a coarse resolution (whole block, 1,000 × 1,000 pixels, 154- × 154-μm image size, 154-nm lateral resolution), while midresolution images (whole block, 8,000 × 8,000 pixels, 161- × 161-μm image size, 20-nm lateral resolution) and high-resolution images (single ommatidium, 4,000 × 4,000 pixels, 21.5- × 21.5-μm image size, 5.4-nm lateral resolution) were

obtained every 5 μm. High-resolution images were sufficiently resolved to view the individual microvilli in all rhabdomeres. Midresolution images were sufficiently resolved to view the coarse orientations of the microvilli in all ommatidia in the block (Fig. 1 *A* and *B*). Thus, the microvilli of a single ommatidium (Fig. 1*C*) were first traced in the high-resolution image stack, and subsequently the same ommatidium was traced in the midresolution stack. The measured orientations matched between the 2 resolutions. The microvillar orientations of all photoreceptors in the block were traced manually in the midresolution stack and registered using a custom routine in MATLAB (MathWorks).

Estimation of the PS_A and Angular Maximum of Sensitivity (ϕ_{max}). The anatomical data were used to calculate the PS_A as an estimate of the physiological photoreceptor PS. The calculations were based on a discrete model (60), modified from ref. 42. A rhabdomere was modeled as a series of 5-μm cylindrical segments, each having a constant and uniform orientation of the microvilli, with orientation angle ϕ_m as measured in the serial sections. Many insect photoreceptors have very high PS (30, 71), which must be based on a high microvillar dichroic ratio D_m. Thus, we assumed $D_m = 10$ (42), independent of wavelength. The incident light was spectrally neutral and randomly polarized. Each segment absorbed a fraction of light, depending on the e-vector angle ϕ; the angle-dependent effective absorption coefficient was

$$\kappa(\phi) = 2\kappa_0\left(1 + (D_m - 1)\cos^2(\phi - \phi_m)\right)(D_m + 1)^{-1}, \quad [1]$$

where the mean absorption coefficient was $\kappa_0 = 0.005\ \mu m^{-1}$ (72–74). Each successive segment was illuminated with the light exiting the preceding segment. To account for the effect of R7, acting as a polarization filter influencing the PS_A of R8, the light exiting R7 was the light flux entering R8. The ratio between the angle-dependent maximum and minimum of the integrated absorption yielded the PS_A of the photoreceptor. The angular maximum of integrated absorption was ϕ_{max}.

Electrophysiology. Horseflies were anesthetized by chilling on ice and glued to a plastic tube with a mixture of beeswax and resin. The tube with the animal was positioned into a miniature goniometer and the preparation was carefully aligned with the eye equator horizontally or vertically, to allow for the different entry points of the microelectrode at the eye's outer lateral, dorsal, or ventral edge. A small hole was cut into the cornea using a razorblade chip and sealed with silicon vacuum grease. The reference electrode was a 50-μm-diameter Ag/AgCl wire, inserted into the margin of the retina. The microelectrodes were pulled from borosilicate or quartz glass capillaries (1-mm/0.5-mm outer/inner diameter) on a P-2000 laser micropipette puller (Sutter) and mounted on a piezo-driven micromanipulator (Sensapex). The microelectrodes were back-filled with 3M KCl, yielding a typical resistance 80 to 120 MΩ for borosilicate and 100 to 200 MΩ for quartz pipettes, respectively. The signal was amplified with a SEC-10LX amplifier (NPI Electronic), conditioned with a Cyber Amp 320 (Axon Instruments) and digitized with a Micro 1401 (CED). The analog signal was low-pass-filtered at 1 kHz with an 8-pole Bessel filter to prevent aliasing and sampled at 2.5 kHz. WinWCP (Strathclyde Electrophysiology Software, version 4.0.5) software was used for data acquisition. Input resistance of photoreceptors was measured by measuring the membrane hyperpolarization during the injection of −0.2 nA in discontinuous current clamp mode at 20 kHz. The outer photoreceptors R1–6 could be held for up to 20 min, while the recordings in the central photoreceptors R7 and R8 lasted only up to 3 to 5 min.

Optical Setup. Two different light sources were used for the stimulation. For precise spectral sensitivity measurements, we used a 75-W XBO lamp with a quartz condenser (Cairn Research), an SH05/M shutter (Thorlabs), a monochromator (B&M Optik) with a bandpass (full width at half maximum, FWHM) of 10 nm or a monochromator (77250-M; Newport Oriel) with a bandpass (FWHM) of 5 nm, a series of reflective neutral density (ND) filters (CVI Melles Griot), and a rotatable and continuously variable ND filter on a fused silica substrate NDC-100C-4 (Thorlabs). The monochromator and the ND filter were driven with stepper motors, controlled by a Due microcontroller (Arduino). For fast intracellular measurements of the spectral sensitivity we invented, assembled, and used a so-called LED synth (75). In short, light from different light-emitting diodes (LEDs) with emission peaks from 350 to 630 nm was combined with a planar diffraction grating, transforming the spectra of various LEDs into bands with uniform bandwidths. The spacing between the 21 equally wide spectral bands was about 15 nm. The combined output beam was directed into a fiber. The outputs from the XBO lamp and the LED synth were combined with a nonpolarizing polka-dot beam splitter (Thorlabs) and projected on the animal's eye through a focusing objective stage, assembled from fused silica lenses (Thorlabs). The optical path was equipped with a field and an aperture diaphragm (Qioptiq) that allowed control of the aperture of the stimulating beam to a half-angle between 1.5° and 15°. The light output was calibrated using a radiometrically calibrated spectrophotometer Flame (Ocean Optics). The degree of polarization (DOP) of the light from the stimulating setup was checked by projecting monochromatic pulses onto an OPT-101 photodiode (Texas Instruments) through an additional polarization filter. The minimal and maximal photodiode voltage within a polarizer 360° cycle was measured and the DOP was calculated. The intrinsic DOP of the light from the XBO was 0; DOP of light from the XBO, passed through the polarizer, was ∼1. The intrinsic DOP of light from the LED synth was continuously varied between 0.3 (300 nm), 0 (at 500 nm), and 0.3 (at 600 nm), and therefore the LED synth was not used for PS measurements. The spectrally dependent DOP of LED light had minor effect on the measured spectral sensitivity of PS cells R7 and R8. Therefore, the LED synth was only used for quick cell identification at the impalement. All subsequent analyses were performed using the XBO light source.

The stimulus–response relation was estimated with a series of light pulses with graded intensity and by fitting the response voltages with a Hill sigmoid function:

$$V(I) = V_0 I^n (R^n + I^n)^{-1}, \quad [2]$$

where R is the intensity needed for half-maximal response, V_0 is the maximal response, and n is the slope of the sigmoid. The effective intensities from the spectral scan were estimated from amplitudes V using the inverse transform of the Hill function:

$$I(\lambda) = R\left[(V_0 - V)^{-1} V\right]^{(1/n)}. \quad [3]$$

The spectral sensitivity was then calculated as the normalized inverse criterion intensity. Sensitivity spectra were obtained by fitting rhodopsin templates (76) to data (R1–6, R7, and R8V) or by smoothing experimental data (R8H).

PS was measured by projecting monochromatic light pulses through a UV-capable polarizer foil OUV2500 (Knight Optical). The polarizer, inserted in the light path after a polka-dot beam splitter, was rotated around its axis in 9° or 18° steps. A horizontally oriented e-vector was defined as 0° and 180° and vertically as 90° and 270° with respect to the eye equator. PS was calculated by transforming the response voltages into sensitivity and fitting the sensitivity values with a squared cosine function:

$$S(\phi_{stim}) = A[\cos(\phi_{stim} - \phi_{max})]^2 + C, \quad [4]$$

where S is the sensitivity, ϕ_{stim} the e-vector angle of the polarizer, A the amplitude, ϕ_{max} the angular PS maximum, and C the offset. PS was then calculated as the ratio between the sensitivity maximum and minimum.

Behavioral Experiments. Spectral and polarization dependence of horsefly polarotactic behavior was tested with artificial horsefly lures with controlled spectral composition of reflected light. The lures were inflatable beach balls (33-cm diameter) (AP731795-10; Anda Ltd.) with a shiny black surface. This allowed us to create multiple identical replicates of a dark body with a polarized shine, which would be very difficult using real animal fur. To create nonshiny lures, the balls were covered with a matte black fabric. The balls were suspended under a square 1- × 1-m frame, 1.5 m from the ground. The frames supported 4-mm-thick polymethylmethacrylate (plexi) plates (Evonik Performance Materials) in combination with different color filters that blocked selected parts of the spectrum of incident light. Full-spectrum light was transmitted through a UV-permeable plexi Sunactive, cutting below 300 nm (transmitting full spectrum, relevant for horsefly vision: UV, blue, and green light, hence labeled UBG). UV light was attenuated with a combination of UV-blocking plexi Clear UV 100 (cutoff at 380 nm) and adhesive window protection foil SCARL 400 (3M, USA), yielding cutoff at 400 nm. UV and blue lights were attenuated with a Lee 101 foil filter; the blue bandpass filter was a Lee 068 foil (LEE Filters); both filters were glued to UV-blocking plexi. Filter transmittances are shown in *SI Appendix*, Fig. S3C. In another set of experiments the balls were illuminated with artificial light sources, powered from a car battery, that allowed independently controlled UV, blue, and green light, incident on the balls. UV light at 370 nm was provided by fluorescent tubes LT 18W/073 Blacklight blue (Narva), while blue (470 nm) and green (525 nm) light was from LED strips (Epistar) having 60 LED per m, consuming 10 W/m of strip. The light sources were mounted in 1- × 1-m wooden boxes that were positioned on the frames instead of the filters.

Each box contained 2 UV tubes, 4 m of the blue and 4 m of the green strip. The inside of the box was dressed with aluminum foil. The irradiance spectra of artificial light sources, measured at the location of the ball, are shown in *SI Appendix*, Fig. S3*D*. The DOP of the stimulus was controlled by the texture of the ball surface. The shiny black surface polarized the light, while the matte surface of the ball diffused and depolarized the reflected light. Finally, a lure having a high DOP and low achromatic contrast was constructed from a celluloid foil (transmittance shown in *SI Appendix*, Fig. S3*C*) in a 40- × 40-cm wooden frame, suspended at 45° in the place of the balls below the UBG filter plate. The degree of polarization of all lures is shown in *SI Appendix*, Fig. S3*A*. Angle of polarization in the different lures did not vary throughout the spectrum and is shown only in the blue channel (*SI Appendix*, Fig. S3*B*). Briefly, the balls reflected light, polarized under all angles, while the celluloid foil only reflected horizontally polarized light.

The field experiments were performed in a hillside meadow in a karstic forest (Global Positioning System coordinates 45.943362 N, 14.449533 E). The area was heavily infested with horseflies, which probably feed on wild animals such as deer. The meadow was surrounded with tall trees that prevented the skylight at low elevations to illuminate the balls from the sides, so that the balls were mostly illuminated by sunlight and skylight, transmitted through the filters. The experiments were carried out in June and July 2016, 2017, and 2018 between noon and 2 PM. The horseflies were lured to 3 to 5 balls at once, positioned at least 100 m apart. The attractiveness of a specific combination of light and ball was estimated from the number of animals visiting the ball. The visits were counted by observers, standing 3 to 4 m from the ball. Each counting session lasted for 15 min and was repeated several times with random rotation of the lures among the different locations. Attraction was expressed as a percentage of the visits to a single lure divided by the total number of visits to all lures during the entire counting session. For instance, in the main experiment (Fig. 3), 14,260 horsefly visits to 5 balls during 12 repeats (12 × 15 min = 3 h) means that each ball was receiving on average one visit every 4 s. Inevitably, single horseflies bumping many times into the same ball were counted multiple times. The lures were visited exclusively by the horseflies, belonging to the *Tabanus* genus: *T. bromius*, *T. bovinus*, and *T. tergestinus*, which was verified with occasional close-up observations and by determining the insects, glued to a ball, coated with Tanglefoot. The counts were tested for normality and analyzed with one-way ANOVA using Bonferroni-corrected multiple comparisons. We used Prism 7.0 (GraphPad) for the analysis and plotting.

ACKNOWLEDGMENTS. This material is based upon work supported by the Air Force Office of Scientific Research, Air Force Materiel Command, US Air Force under Awards FA9550-15-1-0068 and FA9550-19-1-7005. G.B. and M.K. have received funding from the Slovenian Research Agency (Grants P3-0333 to G.B. and 130-2014 to M.K.). P.P. was cofinanced by the European Union from the European Regional Development Fund and by the Ministry of Education, Science and Sport of Slovenia, priority axis "International Competitiveness of Research, Innovation and Technological Development," decision letter 5442-1/2018/434. We thank Armin Zankel for his kind assistance at the serial block-face SEM facility and Drs. Doekele Stavenga, Mathias Wernet, and Mikko Juusola for commenting on the manuscript.

1. R. Wehner, Astronavigation in insects. *Annu. Rev. Entomol.* **29**, 277–298 (1984).
2. T. F. Mathejczyk, M. F. Wernet, "Sensing polarized light in insects" in *Oxford Research Encyclopedias: Neuroscience*, S. M. Sherman, Ed. (Oxford University Press, 2017).
3. M. J. How *et al*., Target detection is enhanced by polarization vision in a fiddler crab. *Curr. Biol.* **25**, 3069–3073 (2015).
4. C. R. Sharkey, J. C. Partridge, N. W. Roberts, Polarization sensitivity as a visual contrast enhancer in the Emperor dragonfly larva, *Anax imperator*. *J. Exp. Biol.* **218**, 3399–3405 (2015).
5. I. Novales Flamarique, Swimming behaviour tunes fish polarization vision to double prey sighting distance. *Sci. Rep.* **9**, 944 (2019).
6. G. Horváth, J. Majer, L. Horváth, I. Szivák, G. Kriska, Ventral polarization vision in tabanids: Horseflies and deerflies (Diptera: Tabanidae) are attracted to horizontally polarized light. *Naturwissenschaften* **95**, 1093–1100 (2008).
7. Á. Egri *et al*., New kind of polarotaxis governed by degree of polarization: Attraction of tabanid flies to differently polarizing host animals and water surfaces. *Naturwissenschaften* **99**, 407–416 (2012).
8. J. E. Chainey, "Horse-flies, deer-flies and clegs (Tabanidae)" in *Medical Insects and Arachnids*, R. P. Lane, R. W. Crosskey, Eds. (Springer, Dordrecht, 1993), pp. 310–332.
9. G. Horváth *et al*., Why do horseflies need polarization vision for host detection? Polarization helps tabanid flies to select sunlit dark host animals from the dark patches of the visual environment. *R. Soc. Open Sci.* **4**, 170735 (2017).
10. R. C. Hardie, "Functional organization of the fly retina" in *Progress In Sensory Physiology*, H. Autrum *et al*., Eds. (Springer, Berlin, 1985), **vol. 5**, pp. 1–79.
11. D. G. Stavenga, Angular and spectral sensitivity of fly photoreceptors. I. Integrated facet lens and rhabdomere optics. *J. Comp. Physiol. A Neuroethol. Sens. Neural Behav. Physiol.* **189**, 1–17 (2003).
12. T. Wolff, D. Ready, "Pattern formation in the *Drosophila* retina" in *The Development of Drosophila Melanogaster*, M. Bate, A. Martinez-Arias, Eds. (Cold Spring Harbor Press, 1993), **vol. 2**, pp. 1277–1325.
13. K. Kirschfeld, Aufnahme und Verarbeitung optischer Daten im Komplexauge von Insekten. *Naturwissenschaften* **58**, 201–209 (1971).
14. J. Rister *et al*., Dissection of the peripheral motion channel in the visual system of *Drosophila melanogaster*. *Neuron* **56**, 155–170 (2007).
15. K.-F. Fischbach, A. Dittrich, The optic lobe of *Drosophila melanogaster*. I. A Golgi analysis of wild-type structure. *Cell Tissue Res.* **258**, 441–475 (1989).
16. A. Huber, D. P. Smith, C. S. Zuker, R. Paulsen, Opsin of *Calliphora* peripheral photoreceptors R1-6. Homology with *Drosophila* Rh1 and posttranslational processing. *J. Biol. Chem.* **265**, 17906–17910 (1990).
17. M. Heisenberg, E. Buchner, The role of retinula cell types in visual behavior of *Drosophila melanogaster*. *J. Comp. Physiol.* **117**, 127–162 (1977).
18. S. Yamaguchi, R. Wolf, C. Desplan, M. Heisenberg, Motion vision is independent of color in *Drosophila*. *Proc. Natl. Acad. Sci. U.S.A.* **105**, 4910–4915 (2008).
19. J. Morante, C. Desplan, The color-vision circuit in the medulla of *Drosophila*. *Curr. Biol.* **18**, 553–565 (2008).
20. S. Gao *et al*., The neural substrate of spectral preference in *Drosophila*. *Neuron* **60**, 328–342 (2008).
21. S. Yamaguchi, C. Desplan, M. Heisenberg, Contribution of photoreceptor subtypes to spectral wavelength preference in *Drosophila*. *Proc. Natl. Acad. Sci. U.S.A.* **107**, 5634–5639 (2010).
22. M. F. Wernet *et al*., Homothorax switches function of *Drosophila* photoreceptors from color to polarized light sensors. *Cell* **115**, 267–279 (2003).
23. C. Schnaitmann, C. Garbers, T. Wachtler, H. Tanimoto, Color discrimination with broadband photoreceptors. *Curr. Biol.* **23**, 2375–2382 (2013).
24. T. J. Wardill *et al*., Multiple spectral inputs improve motion discrimination in the *Drosophila* visual system. *Science* **336**, 925–931 (2012).
25. W. H. Chou *et al*., Identification of a novel *Drosophila* opsin reveals specific patterning of the R7 and R8 photoreceptor cells. *Neuron* **17**, 1101–1115 (1996).
26. N. Franceschini, K. Kirschfeld, B. Minke, Fluorescence of photoreceptor cells observed *in vivo*. *Science* **213**, 1264–1267 (1981).
27. O. Trujillo-Cenóz, G. D. Bernard, Some aspects of the retinal organization of Sympycnus linetaus Loew (Diptera, Dolichopodidae). *J. Ultrastruct. Res.* **38**, 149–160 (1972).
28. H. Ebadi *et al*., Patterning the insect eye: From stochastic to deterministic mechanisms. *PLoS Comput. Biol.* **14**, e1006363 (2018).
29. M. E. Fortini, G. M. Rubin, The optic lobe projection pattern of polarization-sensitive photoreceptor cells in *Drosophila melanogaster*. *Cell Tissue Res.* **265**, 185–191 (1991).
30. R. C. Hardie, Properties of photoreceptor R7 and photoreceptor R8 in dorsal marginal ommatidia in the compound eyes of *Musca* and *Calliphora*. *J. Comp. Physiol.* **154**, 157–165 (1984).
31. T. Labhart, E. P. Meyer, Detectors for polarized skylight in insects: A survey of ommatidial specializations in the dorsal rim area of the compound eye. *Microsc. Res. Tech.* **47**, 368–379 (1999).
32. S. Wada, Spezielle randzonale Ommatidien der Fliegen (Diptera: Brachycera): Architektur und Verteilung in den Komplexaugen. *Z. Morphol. Tiere* **77**, 87–125 (1974).
33. H. L. De Vries, A. Spoor, R. Jielof, Properties of the eye with respect to polarized light. *Physica* **19**, 419–432 (1953).
34. A. W. Snyder, S. B. Laughlin, Dichroism and absorption by photoreceptors. *J. Comp. Physiol.* **100**, 101–116 (1975).
35. T. H. Goldsmith, R. Wehner, Restrictions on rotational and translational diffusion of pigment in the membranes of a rhabdomeric photoreceptor. *J. Gen. Physiol.* **70**, 453–490 (1977).
36. M. F. Moody, J. R. Parriss, The discrimination of polarized light by *Octopus*: A behavioural and morphological study. *Z. Vgl. Physiol.* **44**, 268–291 (1961).
37. R. Wehner, G. D. Bernard, Photoreceptor twist: A solution to the false-color problem. *Proc. Natl. Acad. Sci. U.S.A.* **90**, 4132–4135 (1993).
38. A. Kelber, C. Thunell, K. Arikawa, Polarisation-dependent colour vision in *Papilio* butterflies. *J. Exp. Biol.* **204**, 2469–2480 (2001).
39. M. Kinoshita, K. Yamazato, K. Arikawa, Polarization-based brightness discrimination in the foraging butterfly, *Papilio xuthus*. *Philos. Trans. R. Soc. Lond. B Biol. Sci.* **366**, 688–696 (2011).
40. U. Smola, H. Wunderer, Fly rhabdomeres twist *in vivo*. *J. Comp. Physiol.* **142**, 43–49 (1981).
41. U. Smola, H. Wunderer, Twisting of blowfly (*Calliphora erythrocephala* meigen) (Diptera, calliphoridae) rhabdomeres: An *in vivo* feature unaffected by preparation or fixation. *Int. J. Insect Morphol. Embryol.* **10**, 331–343 (1981).
42. M. F. Wernet *et al*., Genetic dissection reveals two separate retinal substrates for polarization vision in *Drosophila*. *Curr. Biol.* **22**, 12–20 (2012).
43. N. W. Roberts, M. L. Porter, T. W. Cronin, The molecular basis of mechanisms underlying polarization vision. *Philos. Trans. R. Soc. Lond. B Biol. Sci.* **366**, 627–637 (2011).
44. A. W. Snyder, Polarization sensitivity of individual retinula cells. *J. Comp. Physiol.* **83**, 331–360 (1973).
45. H. Wunderer, P. Seifert, F. Pilstl, A. Lange, U. Smola, Crustacean-like rhabdoms at the dorsal rim of several Dipteran eyes (Syrphidae, Tabanidae). *Naturwissenschaften* **77**, 343–345 (1990).

46. H. Wunderer, U. Smola, Functional morphology of the retina of *Chrysops caecutiens* and *Haematopota pluvialis* (Diptera, Tabanidae)–Region around eye equator. *Int. J. Insect Morphol. Embryol.* **15**, 311–319 (1986).
47. P. Seifert, H. Wunderer, U. Smola, Regional differences in a nematoceran retina (Insecta, Diptera). *Zoomorphology* **105**, 99–107 (1985).
48. F. J. Heras, S. B. Laughlin, Optimizing the use of a sensor resource for opponent polarization coding. *PeerJ* **5**, e2772 (2017).
49. L. Schneider, H. Langer, The structure of the rhabdome in the bifunctional compound eye of the pond skater, Gerris lacustris. *Z. Zellforsch Mikrosk. Anat.* **99**, 538–559 (1969).
50. R. Schwind, Zonation of the optical environment and zonation in the rhabdom structure within the eye of the backswimmer, *Notonecta glauca*. *Cell Tissue Res.* **232**, 53–63 (1983).
51. G. Belušič, K. Šporar, A. Meglič, Extreme polarisation sensitivity in the retina of the corn borer moth *Ostrinia*. *J. Exp. Biol.* **220**, 2047–2056 (2017).
52. T. Heinloth, J. Uhlhorn, M. F. Wernet, Insect responses to linearly polarized reflections: Orphan behaviors without neural circuits. *Front. Cell. Neurosci.* **12**, 50 (2018).
53. P. T. Weir *et al*., Anatomical reconstruction and functional imaging reveal an ordered array of skylight polarization detectors in *Drosophila*. *J. Neurosci.* **36**, 5397–5404 (2016).
54. C. Schnaitmann *et al*., Color processing in the early visual system of *Drosophila*. *Cell* **172**, 318–330.e18 (2018).
55. T. Labhart, Polarization-opponent interneurons in the insect visual system. *Nature* **331**, 435–437 (1988).
56. S. Heinze, "Polarization vision" in *Encyclopedia of Computational Neuroscience*, D. Jaeger, R. Jung, Eds. (Springer, New York, 2013), pp. 1–30.
57. J. Rister, C. Desplan, D. Vasiliauskas, Establishing and maintaining gene expression patterns: Insights from sensory receptor patterning. *Development* **140**, 493–503 (2013).
58. M. Hilbrant *et al*., Sexual dimorphism and natural variation within and among species in the *Drosophila* retinal mosaic. *BMC Evol. Biol.* **14**, 240 (2014).
59. D. G. Stavenga, Angular and spectral sensitivity of fly photoreceptors. II. Dependence on facet lens F-number and rhabdomere type in *Drosophila*. *J. Comp. Physiol. A Neuroethol. Sens. Neural Behav. Physiol.* **189**, 189–202 (2003).
60. M. Ilić, A. Meglič, M. Kreft, G. Belušič, The fly sensitizing pigment enhances UV spectral sensitivity while preventing polarization-induced artifacts. *Front. Cell. Neurosci.* **12**, 34 (2018).
61. J. Marshall, N. Roberts, T. Cronin, "Polarisation signals" in *Polarized Light and Polarization Vision in Animal Sciences*, G. Horváth, Ed. (Springer, Heidelberg, 2014), pp. 407–442.
62. D. G. Stavenga, M. F. Wehling, G. Belušič, Functional interplay of visual, sensitizing and screening pigments in the eyes of *Drosophila* and other red-eyed dipteran flies. *J. Physiol.* **595**, 5481–5494 (2017).
63. I. Novales Flamarique, H. I. Browman, Wavelength-dependent polarization orientation in *Daphnia*. *J. Comp. Physiol. A Neuroethol. Sens. Neural Behav. Physiol.* **186**, 1073–1087 (2000).
64. H. Sasaki, Comparison of capturing tabanid flies (Diptera: Tabanidae) by five different color traps in the fields. *Appl. Entomol. Zool.* **36**, 515–519 (2001).
65. S. A. Allan, J. Stoffolano, Effects of background contrast on visual attraction and orientation of *Tabanus nigrovittatus* (Diptera: Tabanidae). *Environ. Entomol.* **15**, 689–694 (1986).
66. R. Mizell, R. F. Mizell Iv, R. A. Mizell, Trolling: A novel trapping method for *Chrysops* spp. (Diptera: Tabanidae). *Fla. Entomol.* **85**, 356–366 (2003).
67. J. M. Lindh *et al*., Optimizing the colour and fabric of targets for the control of the tsetse fly *Glossina fuscipes fuscipes*. *PLoS Negl. Trop. Dis.* **6**, e1661 (2012).
68. R. Hardie, K. Vogt, A. Rudolph, The compound eye of the tsetse-fly (*Glossina morsitans morsitans* and *Glossina palpalis palpalis*). *J. Insect Physiol.* **35**, 423–431 (1989).
69. S. A. Allan, J. F. Day, J. D. Edman, Visual ecology of biting flies. *Annu. Rev. Entomol.* **32**, 297–316 (1987).
70. S. Krčmar, D. K. Hackenberger, B. K. Hackenberger, Key to the horse flies fauna of Croatia (Diptera, Tabanidae). *Period. Biol.* **113**, 1–61 (2011).
71. J. Stalleicken, T. Labhart, H. Mouritsen, Physiological characterization of the compound eye in monarch butterflies with focus on the dorsal rim area. *J. Comp. Physiol. A Neuroethol. Sens. Neural Behav. Physiol.* **192**, 321–331 (2006).
72. K. Kirschfeld, "Absorbtion properties of photopigments in single rods, cones and rhabdomeres" in *International School of Physics "Enrico Fermi": Course XLIII, 1968*, W. Reichhardt, Ed. (Academic Press, 1969), pp. 116–136.
73. W. S. Stark, A. M. Ivanyshyn, R. M. Greenberg, Sensitivity and photopigments of R1-6, a 2-peaked photoreceptor, in *Drosophila, Calliphora* and *Musca*. *J. Comp. Physiol.* **121**, 289–305 (1977).
74. D. G. Stavenga, Fly visual pigments. Difference in visual pigments of blowfly and dronefly peripheral retinula cells. *J. Comp. Physiol.* **111**, 137–152 (1976).
75. G. Belušič, M. Ilić, A. Meglič, P. Pirih, A fast multispectral light synthesiser based on LEDs and a diffraction grating. *Sci. Rep.* **6**, 32012 (2016).
76. D. G. Stavenga, R. P. Smits, B. J. Hoenders, Simple exponential functions describing the absorbance bands of visual pigment spectra. *Vision Res.* **33**, 1011–1017 (1993).